The SAURON project - XVIII. The integrated UV–linestrength relations of early-type galaxies

Martin Bureau,[1*] Hyunjin Jeong,[2] Sukyoung K. Yi,[2†] Kevin Schawinski,[3‡]
Ryan C. W. Houghton,[1] Roger L. Davies,[1] Roland Bacon,[4] Michele Cappellari,[1]
P. Tim de Zeeuw,[5,6] Eric Emsellem,[4,5] Jesús Falcón-Barroso,[7] Davor Krajnović,[5]
Harald Kuntschner,[8] Richard M. McDermid,[9] Reynier F. Peletier,[10] Marc Sarzi,[11]
Young-Jong Sohn,[2] Daniel Thomas,[12] Remco C. E. van den Bosch,[13]
and Glenn van de Ven[13]

[1] *Sub-Department of Astrophysics, University of Oxford, Denys Wilkinson Building, Keble Road, Oxford OX1 3RH, U.K.*
[2] *Department of Astronomy, Yonsei University, Seoul 120-749, Korea*
[3] *Department of Physics, Yale University, New Haven, CT 06511, U.S.A.;*
Yale Center for Astronomy and Astrophysics, P.O. Box 208121, New Haven, CT 06520, U.S.A
[4] *Université de Lyon 1, CRAL, Observatoire de Lyon, 9 av. Charles André, F-69230 Saint-Genis Laval; CNRS, UMR 5574;*
ENS de Lyon, France
[5] *European Southern Observatory, Karl-Schwarzschild-Str. 2, 85748 Garching, Germany*
[6] *Leiden Observatory, Leiden University, Niels Bohrweg 2, 2333 CA Leiden, The Netherlands*
[7] *Instituto de Astrofísica de Canarias, Vía Láctea s/n, La Laguna, Tenerife, Spain;*
Departamento de Astrofísica, Universidad de La Laguna (ULL), E-38205 La Laguna, Tenerife, Spain
[8] *Space Telescope European Coordinating Facility, European Southern Observatory, Karl-Schwarzschild-Str. 2, 85748 Garching, Germany*
[9] *Gemini Observatory, 670 North A'Ohoku Place, Hilo, Hawaii 96720, U.S.A.*
[10] *Kapteyn Astronomical Institute, University of Groningen, P.O. Box 800, 9700 AV Groningen, The Netherlands*
[11] *Centre for Astrophysics Research, University of Hertfordshire, Hatfield, U.K.*
[12] *Institute of Cosmology and Gravitation, Mercantile House, Hampshire Terrace, University of Portsmouth, Portsmouth PO1 2EG, U.K.*
[13] *Max Planck Institute for Astronomy, D-69117 Heidelberg, Germany*

4 February 2011

ABSTRACT

Using far (FUV) and near (NUV) ultraviolet photometry from guest investigator programmes on the *Galaxy Evolution Explorer* (*GALEX*) satellite, optical photometry from the MDM Observatory and optical integral-field spectroscopy from SAURON, we explore the UV–linestrength relations of the 48 nearby early-type galaxies in the SAURON sample. Identical apertures are used for all quantities, avoiding aperture mismatch. We show that galaxies with purely old stellar populations show well-defined correlations of the integrated $FUV-V$ and $FUV-NUV$ colours with the integrated $Mg\,b$ and $H\beta$ absorption linestrength indices, strongest for $FUV-NUV$. Correlations with the $NUV-V$ colour, Fe5015 index and stellar velocity dispersion σ are much weaker. These correlations put stringent constraints on the origin of the UV-upturn phenomenon in early-type galaxies, and highlight its dependence on age and metallicity. In particular, despite recent debate, we recover the negative correlation between $FUV-V$ colour and Mg linestrength originally publicised by Burstein et al. (1988), which we refer to as the "Burstein relation", suggesting a positive dependence of the UV-upturn on metallicity. We argue that the scatter in the correlations is real, and present mild evidence that a strong UV excess is preferentially present in slow-rotating galaxies. We also demonstrate that most outliers in the correlations are galaxies with current or recent star formation, some at very low levels. We believe that this sensitivity to weak star formation, afforded by the deep and varied data available for the SAURON sample, explains why our results are occasionally at odds with other recent but shallower surveys. This is supported by the analysis of a large, carefully-crafted sample of more distant early-type galaxies from the Sloan Digital Sky Survey (SDSS), more easily comparable with current and future large surveys.

Key words: galaxies: elliptical and lenticular, cD – galaxies: evolution – galaxies: photometry – galaxies: stellar content – galaxies: structure – ultraviolet: galaxies

1 INTRODUCTION

Far-ultraviolet (FUV) radiation was first discovered in early-type galaxies by the *Orbiting Astronomical Observatory-2* in 1969 (Code et al. 1972). It was rapidly realised that, below ≈ 2000 Å, many early-types show spatially extended *rising* flux for decreasing wavelengths (e.g. Code & Welch 1979; Bertola et al. 1980), a surprising behaviour for presumably old stellar populations. This spawned a debate on the origin of this UV upturn that continues to this day.

The leading hypothesis suggests that this flux is due to hot stars on an extreme horizontal branch (EHB) and their progeny (e.g. asymptotic giant branch (AGB) stars manqué), either metal-poor (e.g., Lee, Demarque & Zinn 1994; Park & Lee 1997; see also Buzzoni & González-Lópezlira 2008) or metal-rich (e.g. Greggio & Renzini 1990; Horch, Demarque & Pinsonneault 1992; Bressan, Chiosi & Fagotto 1994; Dorman, O'Connell & Rood 1995; Yi, Demarque & Kim 1997), with possible significant effects from He enhancement (e.g. Lee et al. 2005b; Kaviraj et al. 2007). Binary star systems offer another compelling possibility, with limited dependence on age and metallicity (e.g. Maxted et al. 2001; Han et al. 2003; Han, Podsiadlowski & Lynas-Gray 2007). Post-AGB (PAGB) stars in the planetary nebula stage also emit FUV radiation, but they are generally thought to be too hot, too few and to have too short a lifetime to explain the observed fluxes alone (e.g. Greggio & Renzini 1990; Dorman et al. 1995; Brown et al. 1997). Clearly, very young stars in star-forming galaxies can also emit in the FUV (see, e.g., Ferreras & Silk 2000; Yi et al. 2005), but they necessarily have evolving properties (e.g. characteristic temperature of the UV spectrum), they have different spectral signatures from those normally observed in UV-upturn galaxies (e.g. strong C IV lines) and they are expected to be clumpy, none of which is supported by observations. A thorough review of these issues is available in O'Connell (1999), while Brown (2004) and Yi (2008) provide more recent but shorter overviews. See Heber (2009) for a review of hot subdwarf stars.

In addition to its roughly constant spectral slope ($T_{\rm eff} \approx 20,000$ K; Brown et al. 1997), one of the main constraints on the possible origins of the UV upturn is its systematic dependence on bulk galaxy properties. Although mentioned in Faber (1983), Burstein et al. (1988, hereafter BBBFL88) are generally considered the first to have systematically investigated the dependence of the UV upturn on the stellar population and dynamical properties of a large sample of early-type galaxies. BBBFL88 found clear non-linear correlations of the UV-optical colours with both the absorption linestrength index Mg_2 (see Faber et al. 1985) and the central stellar velocity dispersion σ. In memory of David Burstein and in view of the long-lasting impact of BBBFL88, we will hereafter refer to the former correlation as the "Burstein relation". These correlations have formed the basis of much of the observational and theoretical work on the UV upturn to date. Crucially, contrary to broadband optical and near-infrared colours, the Mg_2 linestrength was found to be stronger for *bluer* UV-optical colours, i.e. galaxies become bluer with increasing metallicity in the UV. Globular clusters show different correlations, pointing to a slightly different origin for the UV radiation (e.g. Dorman et

‡ Einstein Fellow.

al. 1995; Sohn et al. 2006; but see also Lee, Gim & Casetti-Dinescu 2007).

The recent availability of large-area, deep UV imaging from the *Galaxy Evolution Explorer* (*GALEX*) satellite has added another layer of complexity to the problem. Observations of large samples of early-type galaxies from the Sloan Digital Sky Survey (SDSS) have revealed that a very large fraction of them (over 30%) have remarkably strong near-ultraviolet (NUV) and FUV emission. Yi et al. (2005) initially concluded that the majority of UV-blue early-type galaxies were inconsistent with exhibiting a classic UV upturn, and more likely experienced residual star formation. Schawinski et al. (2007) and Kaviraj et al. (2007) elaborated on this with larger samples, the main conclusion being that residual star formation of a few percent of the stellar mass is very common among early-type galaxies. The UV emission regularly found in early-type galaxies is simply too powerful to be accounted for by any current model of the UV upturn, and is far more powerful than anything found in traditional UV-upturn galaxies such as NGC 1399 and NGC 4552.

Some recent work has also thrown the results of BBBFL88 into doubt. In particular, for a very large sample of local early-type galaxies with *GALEX* UV imaging and SDSS optical spectroscopy, Rich et al. (2005) report no correlation of the FUV$-r$ colour against either the metallicity-sensitive Mg_2 and D4000 indices or the stellar velocity dispersion, even after attempting to remove non-early-type and star-forming galaxies from their sample. If anything, a slight correlation opposite to the Burstein relation is observed. Deharveng, Boselli & Donas (2002) report similar findings, although without active galactic nucleus (AGN) or star-formation cuts and using a UV filter centred on 2000 Å, where the UV upturn phenomenon may not dominate. Using data on nearby galaxies but sorting according to morphological type, Donas et al. (2007) do find correlations for elliptical galaxies but those for lenticulars are weak at best, with much scatter and many outliers. Boselli et al. (2005) recover weak correlations analogous to those of BBBFL88 for Virgo Cluster early-type members, but it is unclear whether the correlations extend to low-luminosity systems. If these recent results prove to be robust, much of the theoretical work on the UV upturn will need to be revised, particularly its dependence on metallicity.

To sort out possible discrepancies between the above, as much information as possible is required on the sample galaxies under consideration, particularly regarding possible low-level star formation. We thus consider two samples here. First, the SAURON sample of 48 nearby elliptical and lenticular galaxies (see Table 1; de Zeeuw et al. 2002, hereafter Paper II), for which detailed integral-field maps of the stellar kinematics (Emsellem et al. 2004, hereafter Paper III), stellar absorption linestrengths and populations (Kuntschner et al. 2006, hereafter Paper VI; Kuntschner et al. 2010, hereafter Paper XVII) and ionised gas distribution and kinematics (Sarzi et al. 2006, hereafter Paper V; Sarzi et al. 2010, hereafter Paper XVI) are available, along with detailed dynamical modeling (e.g. Cappellari et al. 2006, 2007; Emsellem et al. 2007, hereafter Paper IV, Paper X and Paper IX, respectively). The molecular gas content (Combes, Young & Bureau 2007; Crocker et al. 2010), UV emission (Jeong et al. 2009, hereafter Paper XIII) and mid-infrared (MIR) emission (Temi, Brighenti & Mathews 2009; Shapiro

et al. 2010, hereafter Paper XV) of the SAURON sample have also been investigated, to more directly probe its star formation properties. Second, we construct a SDSS sample similar to those of Rich et al. (2005) and Donas et al. (2007), but apply much more stringent cuts to remove star-forming galaxies and low quality data. In both cases, we recover the relationships originally suggested by BBBFL88 for the non-star-forming (i.e. quiescent) galaxies only, while including galaxies with even a very low level of star formation considerably blurs the relations or can even give rise to trends in the opposite sense.

In Section 2, we present the photometric and spectroscopic data and related analysis. Section 3 presents the UV–linestrength relations for the SAURON sample while Section 4 discusses the effects of star formation on them. The SDSS sample is presented and discussed in Section 5. We bring all our results together in Section 6 and conclude briefly in Section 7.

2 OBSERVATIONS AND DATA REDUCTION

Although spatially-resolved data provide in principle a more powerful discriminant of UV-upturn theories, we focus here on integrated quantities as they provide a link with past work (particularly BBBFL88) and offer a crucial benchmark for future studies at high redshifts. The latter in particular are essential to probe the evolution of the UV-upturn with look-back time (and thus turnoff mass), an important test of single versus binary stellar origins (see, e.g., Yi et al. 1999; Lee et al. 2005a; Ree et al. 2007). The two-dimensional nature of the SAURON data will be more fully exploited in a companion paper (Jeong et al., in preparation).

Paper VI showed that, to first order, iso-index contours follow a galaxy light (although they are slightly flatter than the isophotes for $Mg\,b$ in $\approx 40\%$ of the cases). We therefore adopt elliptical apertures to measure integrated quantities throughout this paper. We will generally refer to quantities (magnitudes and linestrengths) integrated within ellipses of semi-major axis $R_e/2$, where R_e is the effective radius of the galaxy (i.e. the radius of the aperture encompassing half the galaxy light). A radius of $R_e/2$ is ideal for our work as it is large enough to accurately represent global values, yet it is small enough that the corresponding elliptical apertures are fully covered by the SAURON field-of-view (FOV) for most objects ($\approx 80\%$). Other interesting radii include $R_e/8$ (i.e. central values) and R_e (global values), although the latter requires a small extrapolation for $\approx 60\%$ of the objects.

2.1 UV photometry

All 48 SAURON early-type galaxies except seven were observed in FUV (1350–1750 Å) and/or NUV (1750–2750 Å) with the Medium imaging mode of *GALEX* (see Martin et al. 2005; Morrissey et al. 2005). A total of 17 galaxies were observed as part of our own UV imaging survey of the SAURON sample (*GALEX* guest investigator programmes GI1_109 and GI3_041) and another 17 as part of the *GALEX* team Nearby Galaxy Survey (NGS; Gil de Paz et al. 2005). All these objects were observed for at least one orbit (typically 1500–1700 s) and have excellent data for any aperture up to R_e.

Table 1. SAURON sample data

Galaxy	FUV$_{Re/2}$ (mag)	NUV$_{Re/2}$ (mag)	$V_{Re/2}$ (mag)	$E(B-V)$ (mag)	Mg$b_{Re/2}$ (Å)	Fe5015$_{Re/2}$ (Å)	H$\beta_{Re/2}$ (Å)	σ_e (km s^{-1})	Survey
(1)	(2)	(3)	(4)	(5)	(6)	(7)	(8)	(9)	(10)
NGC0474	19.46 ± 0.18	17.92 ± 0.07	12.70 ± 0.05	0.034	3.65	4.65	1.87	142	N
NGC0524	18.17 ± 0.21	16.99 ± 0.12	11.21 ± 0.03	0.083	4.22	5.07	1.60	225	G
NGC0821	18.96 ± 0.26	17.40 ± 0.10	11.88 ± 0.03	0.110	3.90	4.54	1.71	182	G
NGC1023	17.45 ± 0.07	16.19 ± 0.04	10.61 ± 0.02	0.061	4.26	4.85	1.62	165	N
NGC2695	19.17 ± 0.08	18.28 ± 0.06	12.87 ± 0.04	0.018	4.08	4.17	1.41	184	G
NGC2699	19.98 ± 0.10	18.91 ± 0.05	13.31 ± 0.05	0.020	3.75	4.74	1.87	123	G
NGC2768	18.15 ± 0.16	16.82 ± 0.08	11.25 ± 0.04	0.044	3.81	4.40	1.70	200	N
NGC2974	18.54 ± 0.07	17.64 ± 0.05	12.10 ± 0.04	0.054	4.23	4.84	1.77	227	G
NGC3032	16.53 ± 0.01	15.79 ± 0.02	13.25 ± 0.05	0.017	1.79	3.60	4.46	90	G
NGC3156	18.70 ± 0.22	17.36 ± 0.08	13.35 ± 0.03	0.034	1.79	3.47	3.39	66	A
NGC3414	18.01 ± 0.24	17.02 ± 0.10	12.03 ± 0.03	0.024	3.97	4.43	1.61	191	A
NGC3489	18.24 ± 0.10	16.56 ± 0.03	11.81 ± 0.02	0.017	2.49	4.32	2.74	99	A
NGC3608	18.26 ± 0.40	17.10 ± 0.16	12.02 ± 0.04	0.021	3.90	4.62	1.73	167	A
NGC4150	18.73 ± 0.04	17.46 ± 0.02	13.01 ± 0.03	0.018	2.26	3.81	3.22	77	N
NGC4262	19.50 ± 0.08	18.74 ± 0.04	13.37 ± 0.02	0.035	4.15	4.40	1.54	164	A
NGC4278	17.01 ± 0.03	16.40 ± 0.03	11.29 ± 0.02	0.029	4.42	4.34	1.56	217	N
NGC4374	16.52 ± 0.07	15.54 ± 0.05	10.19 ± 0.03	0.040	4.27	4.54	1.52	261	N
NGC4387	20.20 ± 0.14	18.66 ± 0.06	13.22 ± 0.02	0.033	3.72	4.40	1.69	98	N
NGC4458	20.21 ± 0.26	18.40 ± 0.08	13.07 ± 0.05	0.024	3.36	3.84	1.71	83	N
NGC4459	17.64 ± 0.06	16.41 ± 0.04	11.41 ± 0.03	0.046	3.60	4.54	2.02	155	G
NGC4473	18.35 ± 0.06	17.09 ± 0.03	11.45 ± 0.02	0.028	4.18	4.76	1.62	186	N
NGC4477	18.09 ± 0.11	16.87 ± 0.06	11.46 ± 0.04	0.032	4.00	4.69	1.67	147	N
NGC4486	15.12 ± 0.06	14.59 ± 0.07	9.76 ± 0.04	0.022	4.74	4.38	1.27	268	N
NGC4526	17.59 ± 0.05	16.12 ± 0.03	11.04 ± 0.03	0.022	4.23	4.82	1.77	214	G
NGC4546	18.87 ± 0.07	17.41 ± 0.04	11.70 ± 0.03	0.034	4.18	4.60	1.63	189	N
NGC4550	19.08 ± 0.05	18.02 ± 0.03	13.18 ± 0.02	0.039	3.03	4.18	2.14	103	N
NGC4552	16.45 ± 0.02	16.03 ± 0.03	11.05 ± 0.02	0.041	4.60	5.07	1.58	233	N
NGC4564	18.15 ± 0.04	17.45 ± 0.03	12.27 ± 0.04	0.035	4.24	4.92	1.67	150	N
NGC4570	18.85 ± 0.04	17.67 ± 0.03	12.18 ± 0.03	0.022	4.11	4.67	1.56	167	G
NGC4621	17.26 ± 0.05	16.27 ± 0.04	10.94 ± 0.04	0.033	4.30	4.64	1.56	200	G
NGC4660	19.21 ± 0.23	17.90 ± 0.08	12.41 ± 0.02	0.033	4.24	4.70	1.59	181	A
NGC5198	19.31 ± 0.10	18.42 ± 0.07	13.06 ± 0.03	0.023	4.13	4.65	1.64	173	G
NGC5308	20.41 ± 0.08	19.21 ± 0.04	13.49 ± 0.02	0.018	4.34	4.78	1.58	201	G
NGC5813	18.25 ± 0.16	17.07 ± 0.09	11.87 ± 0.05	0.057	4.26	4.66	1.64	210	G
NGC5831	19.09 ± 0.18	17.64 ± 0.09	12.30 ± 0.04	0.059	3.59	4.66	1.89	148	G
NGC5838	18.47 ± 0.08	17.30 ± 0.04	12.05 ± 0.03	0.053	4.25	4.85	1.68	232	G
NGC5845	19.99 ± 0.08	18.86 ± 0.04	13.29 ± 0.05	0.053	4.36	4.96	1.65	237	N
NGC5846	17.02 ± 0.14	16.20 ± 0.10	11.11 ± 0.05	0.055	4.54	4.78	1.42	213	N
NGC5982	18.55 ± 0.06	17.66 ± 0.04	12.31 ± 0.03	0.018	4.13	5.05	1.74	223	G
NGC7332	21.91 ± 0.79	18.70 ± 0.10	12.78 ± 0.01	0.037	3.33	4.97	2.29	125	A
NGC7457	19.32 ± 0.42	16.99 ± 0.10	11.98 ± 0.04	0.052	2.83	4.36	2.36	75	G

Columns: (2)–(4) and (6)–(8): Quantities integrated within elliptical apertures of semi-major radii $R_e/2$; (2)–(4) have been corrected for Galactic extinction using (5) and the errors are based on Poisson statistics and our sky subtraction. The adopted formal random error on the values in (6)–(8) is 0.1 Å (see Paper VI). (9) Effective stellar velocity dispersion within R_e from Paper XVII, with an adopted error of 5%. (10) Origin of data: A=All-sky Imaging Survey, G=own guest investigator programmes, N=Nearby Galaxy Survey.

The remaining 7 galaxies have only short exposures (typically 100–150 s) from the *GALEX* team All-sky Imaging Survey (AIS; see Martin et al. 2005), and magnitudes integrated within R_e are less reliable. The resulting sample is listed in Table 1. The data reduction, analysis and products are described more fully in a separate paper (Paper XIII), so we only summarise our processing here.

We used the pre-processed images delivered from the *GALEX* pipeline but performed our own sky subtraction by measuring the background level in source-free regions of the images. The spatial resolution is roughly 4″.5 and 6″.0 FWHM at FUV and NUV, respectively, sampled with 1″.5 × 1″.5 pixels. To avoid spurious colour gradients (especially in the inner parts), we thus convolved the FUV data to the spatial resolution of the NUV observations before any analysis.

We carried out surface photometry by measuring the surface brightness within elliptical annuli in the standard manner, using the ELLIPSE task in IRAF (Image Reduction and Analysis Facility). To derive accurate colours, the ellipses were fitted to the NUV images only (with the better signal-to-noise ratio S/N), and those ellipses were then imposed on the FUV images. Photometric zero-points were taken from Morrissey et al. (2005) and the data were corrected for Galactic extinction using the extinction law of Cardelli, Clayton & Mathis (1989). We take the $E(B-V)$

value for each galaxy as tabulated in the NASA/IPAC Extragalactic Database (NED) from Schlegel, Finkbeiner & Davis (1998). For this paper, only the FUV and NUV surface brightness profiles integrated within $R_e/2$ are discussed, but we have checked that analogous results stand with apertures of $R_e/8$ and R_e. The integrated UV magnitudes corrected for Galactic extinction are listed in Table 1, along with errors based on Poisson statistics and our sky subtraction (all UV magnitudes are AB magnitudes).

2.2 Optical photometry

Optical images in the *Hubble Space Telescope* (*HST*) filter F555W (similar to Johnson *V*) were obtained for the entire SAURON sample using the MDM Observatory 1.3-m McGraw-Hill Telescope over several observing runs in 2002–2005. The field-of-view of the MDM images is $17.'3 \times 17.'3$ with $0.''508 \times 0.''508$ pixels, permitting excellent sky subtraction and proper sampling of the seeing. The MDM observations are described in Falćon-Barroso et al. (in preparation). They were reduced in the standard manner in IRAF. The photometric calibration was obtained by observing photometric standard stars from Landolt (1992) over a range of air masses, resulting in a systematic calibration uncertainty of 0.03 mag. Like the FUV data, the MDM images were convolved to the spatial resolution of the NUV data before any analysis.

Again like the FUV data, the surface brightness profiles for the MDM data were measured only after imposing the NUV ellipses, ensuring accurate UV–optical colours. Magnitudes integrated within elliptical apertures of semi-major axis $R_e/2$ (identical to the UV apertures) were then calculated and corrected for Galactic extinction. The integrated and corrected *V* magnitudes (and errors) are listed in Table 1.

2.3 SAURON linestrengths and kinematics

All linestrength measurements come from the SAURON data published in Paper VI, updated in Paper XVII. The observations and data reduction were thoroughly discussed there and will not be repeated here. While BBBFL88 strived to derive integrated *V* magnitudes within apertures equivalent to the roughly $11'' \times 22''$ rectangular aperture of the *International Ultraviolet Observer* (*IUE*), they had no choice but to use essentially central measurements from slit spectroscopy for Mg_2 and σ. A significant improvement in the current work is that integral-field spectroscopy allows us to measure linestrength indices over exactly the same apertures as the UV and optical photometry.

Paper XVII lists linestrength values integrated within circular apertures of radii $R_e/8$ and R_e, but we again use here NUV-defined elliptical apertures of semi-major axes $R_e/2$, as done in Sections 2.1 and 2.2, to avoid potential aperture mismatch problems. We use simple luminosity-weighted linestrength averages of all the bins within the apertures. The resulting integrated linestrength values are listed in Table 1. While not formally equivalent, we show in Appendix A that these measurements are as robust as those obtained by summing the spectra of all the bins concerned and rederiving the linestrengths from scratch. We therefore

adopt the same uncertainty for our integrated linestrengths as Paper XVII, a formal random error of 0.1 Å (maximum) for all measurements.

Since linestrengths are known to correlate with the central velocity dispersion of galaxies (e.g. Terlevich et al. 1981; Burstein et al. 1988; Bernardi et al. 2003), following BBBFL88 we also explore the dependence of the UV–optical colours on σ. For that, we do not use central velocity dispersion measurements as is usually done, but rather again use properly integrated measurements obtained by summing all the spectra within a given aperture, and re-measuring the stellar kinematics (assuming a pure Gaussian line-of-sight velocity distribution (LOSVD), i.e. no high order Gauss-Hermite terms). Such stellar velocity dispersion measurements are already available in Paper IV (updated in Paper XVII) for a circular aperture of radius R_e, and the extrapolation required when the field-of-view of SAURON does not fully cover R_e is detailed there. The resulting "effective" stellar velocity dispersion σ_e is truly the luminosity-weighted second moment of the LOSVD within R_e, and is a good approximation to the second velocity moment which appears in the virial equation. Integrated velocity dispersions only weakly depend on the aperture used, so we do not re-calculate new values for the elliptical apertures used throughout this paper, but instead simply adopt the values and uncertainties listed in Paper XVII (see Table 1).

3 UV RELATIONS

When exploring possible correlations between stellar absorption linestrengths and broadband photometry, our main advantage over all previous studies, including BBBFL88, Rich et al. (2005) and Donas et al. (2007), is the availability not only of UV imaging, but most importantly of integral-field spectroscopy for all targets. All photometric and spectroscopic measurements are thus made on identical apertures, as described in Section 2.

Figure 1 shows the distance-independent correlations between the FUV−*V* colour and the linestrength indices Mg *b*, Fe5015 and Hβ. Although the transformation of Mg *b*, Fe5015 and Hβ to stellar age, metallicity and α-element (over-)abundance is model dependent, Hβ is primarily a tracer of age. For the range of metallicities present in early-type galaxies and considering various stellar population synthesis models (e.g. Thomas et al. 2003; Schiavon 2007), an Hβ linestrength of 1.8 Å corresponds to single stellar population luminosity-weighted ages of roughly 5 to 10 Gyrs (see, e.g., Figure 3 in Paper XVII). This linestrength value thus represents a good choice to separate young from old galaxies, or rather primarily old galaxies with a significant amount of recent star formation and young stars from primarily old galaxies with no or a minimal additional young stellar population. Changing this threshold value slightly does not significantly affect any of our results. To highlight the effects of recent star formation in Figure 1, galaxies with H$\beta > 1.8$ Å, that are inconsistent with a purely old stellar population, are therefore plotted as crosses. Galaxies with no or minimal (in a luminosity-weighted sense) young stellar populations (H$\beta \leqslant 1.8$ Å) are plotted as filled circles.

There is no physical reason why a linear relation should exist between linestrengths and UV excess, but linear fits to

Table 2. Parameters of the best-fit linear UV–linestrength relations for old galaxies only

Colour (mag)	Line (Å)	Slope (Å mag⁻¹)	Zero-point (Å)	Scatter (Å)
FUV−V	Mg b	-0.40 ± 0.09	6.75 ± 0.57	0.15
	Fe	-0.07 ± 0.11	5.11 ± 0.75	0.22
	Hβ	0.12 ± 0.05	0.83 ± 0.32	0.08
FUV−NUV	Mg b	-0.64 ± 0.12	4.89 ± 0.14	0.15
	Fe	-0.21 ± 0.17	4.89 ± 0.19	0.21
	Hβ	0.20 ± 0.08	1.40 ± 0.09	0.07

the data with $H\beta \leqslant 1.8$ Å are shown as solid lines to guide the eye. The value of the correlation coefficient is reported in the bottom right corner of each panel, and the parameters of the best-fit lines are reported in Table 2, all taking errors properly into account. Lastly, the symbols are colour-coded according to the effective stellar velocity dispersion σ_e, increasing from purple to red (Paper XVII).

3.1 Burstein relation: FUV−V vs. Mg b

The top panel of Figure 1 shows the (FUV−V)–Mg b relation, analogous to the (1550−V)–Mg₂ relation discussed by BBBFL88, although both the FUV filter and the Mg index are slightly different and we use a common aperture of $R_e/2$. This is thus our own version of the Burstein relation. Reassuringly, we see a very similar trend. Most importantly, there is a clear correlation between the FUV−V colour and the Mg b linestrength for galaxies with no significant young stellar population ($H\beta \leqslant 1.8$ Å, i.e. quiescent galaxies). This is the systematic variation of the hot component of old stellar populations discovered by BBBFL88. Galaxies with a substantial young stellar population ($H\beta > 1.8$ Å) blur the relation and are found at systematically lower Mg b values, although over a wide range of FUV−V colour.

Given the above, is our (FUV−V)–Mg b relation merely similar to the original Burstein relation or is it identical? In Figure 2, we have strived to transform the data of BBBFL88 to our own parameters. First, using the *IUE* spectra of BBBFL88, we calculated the 1550−FUV colour of NGC 221 and NGC 4649. To calculate the *GALEX* FUV magnitude of every galaxy in BBBFL88's sample, we then simply assumed that each galaxy had one of two spectral shapes: either a normal early-type galaxy spectrum like NGC 221, or a UV upturn spectrum like that of NGC 4649. The *GALEX* FUV magnitudes were then simply obtained by FUV=1550−(1550−FUV)ₙGC221,4649, using (1550−FUV)ₙGC221 for galaxies with (1550−V)≥ 3.4 (normal galaxies) and (1550−FUV)ₙGC4649 for galaxies with (1550−V)< 3.4 (UV upturn galaxies). As the *IUE* apertures of BBBFL88 are not that different from our own, we do not correct the photometry for aperture mismatch. Second, we converted BBBFL88's Mg₂ index measurements into Mg b using the Thomas, Maraston & Bender (2003) stellar population synthesis models, assuming an α-element (over-)abundance [α/Fe]=0.3 for all galaxies. As those Mg₂ values are central, however, we also need to correct the linestrengths for aperture mismatch. To do this, we simply compared the transformed BBBFL88 Mg b values with ours for the 6 galaxies in common (NGC 2768, NGC 4278,
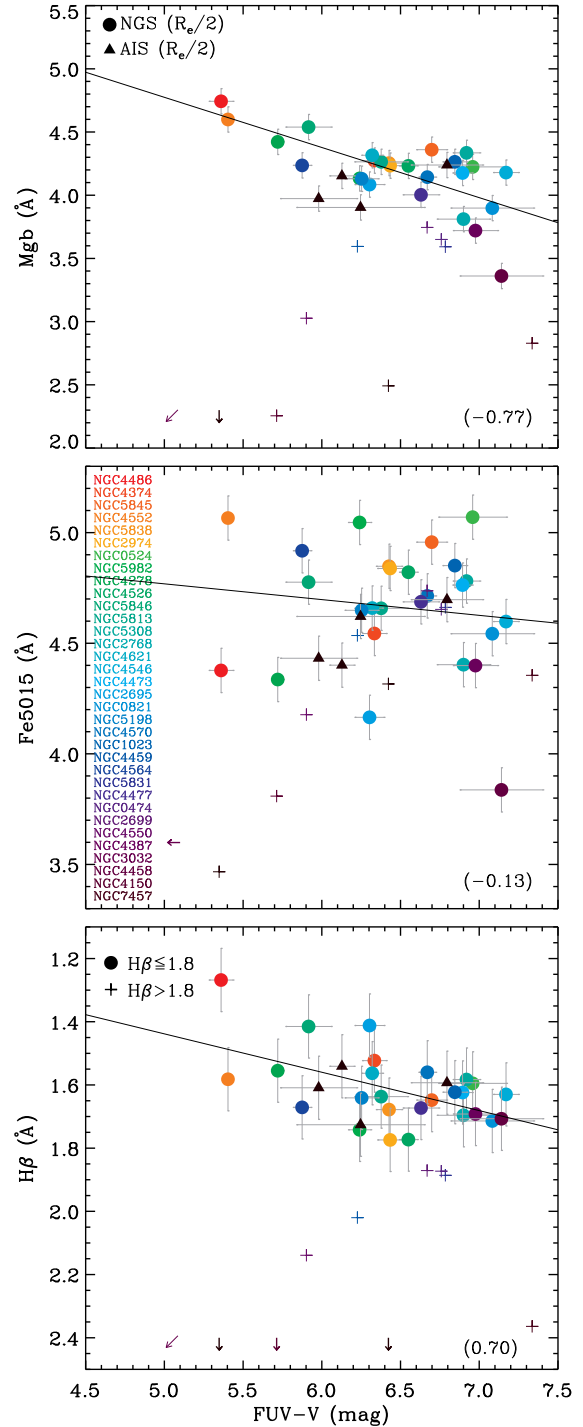
Figure 1. UV upturn dependence on stellar absorption linestrengths. The Mg b (*top*), Fe5015 (*middle*) and Hβ (*bottom*) linestrengths are shown as a function of the FUV−V colour, all integrated within $R_e/2$. The top plot is our own version of the Burstein relation. Objects inconsistent with a purely old stellar population (Hβ> 1.8 Å) are plotted as crosses, others as filled circles. The location of data points lying outside the figure boundaries is indicated by arrows. Note the inverted Hβ axis. Linear fits to the data with $H\beta \leqslant 1.8$ Å are shown as solid lines to guide the eye, and the correlation coefficient is reported in the bottom right corner of each panel. The best-fit parameters are listed in Table 2. The colour table traces the effective stellar velocity dispersion σ_e, from purple at small dispersions through green and red at high dispersions.
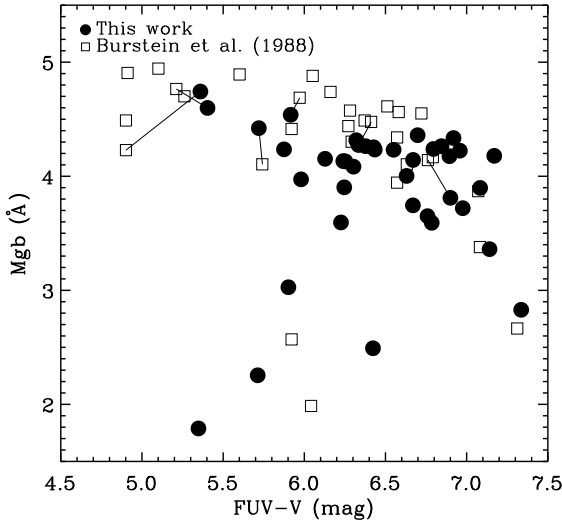
Figure 2. (FUV−V)–Mg b (i.e. Burstein) relation for both our data (filled circles) and the 1550 Å and Mg$_2$ data of BBBFL88 (open squares). The latter have been transformed to FUV and Mg b as discussed in the text. Galaxies in common between the two samples are connected by a solid line. Error bars have been omitted for clarity. The two datasets are consistent, with similar scatter.

NGC 4374, NGC 4486, NGC 4552, NGC 5846), and then applied an average offset to all the galaxies (ΔMg b= 0.52 Å).

The conversion of BBBFL88's data to our own parameters is necessarily very approximate, but Figure 2 shows that our results are consistent with those of BBBFL88. Using much improved data and measuring methods, we have thus recovered the original Burstein relation. Somewhat disappointingly, however, the scatter of our data is about the same. The scatter is also larger than our measurement errors, which suggests that it is real. We explore possible reasons why other studies did not recover the Burstein relation in Sections 4 and 5.

3.2 FUV−V vs. Fe5015

The middle panel of Figure 1 shows the relation of FUV−V with Fe5015. The scatter is very large and a correlation analogous to that of FUV−V vs. Mg b is not obviously present. This is perhaps not surprising, since the correlation of Mg b with the stellar velocity dispersion σ is also much stronger than that of Fe5015. Equally unsurprising then, to our knowledge this correlation has not been discussed much if at all in the literature. Interestingly, however, galaxies with a young population now appear both below and slightly above the best fit to the purely old objects (especially for the smaller $R_e/8$ apertures that are not shown here).

3.3 FUV−V vs. Hβ

The bottom panel of Figure 1 shows the relation of FUV−V with Hβ, which is primarily influenced by age. Separating young and old galaxies in this diagram is somewhat artificial, since we use Hβ itself as our age tracer, but it is striking that a tight correlation is again only present amongst the galaxies with an old stellar population.

Having said that, the observed variation of Hβ with FUV−V is expected from the metallicity dependence of the latter (as traced e.g. by the (FUV−V)–Mg b correlation). It thus does not automatically imply an age dependence.

3.4 NUV−V

Similarly to Figure 1, Figure 3 shows the correlations between the NUV−V colour and the Mg b, Fe5015 and Hβ linestrength indices. The contrast between Figure 1 and 3 is however striking. First, the NUV−V colour range is only about half that in FUV−V for old galaxies. Second, even when considering only old galaxies, the UV–linestrength correlations have essentially disappeared. Third, the galaxies with a young stellar component are much more discrepant. We also point out that nearly all galaxies with very blue NUV−V colours also have high Hβ linestrengths (as expected from star formation), although the opposite is not always true.

Although present across the NUV filter, the UV upturn phenomenon usually clearly dominates the spectral energy distribution only at wavelengths blueward of 2000 Å. It thus cannot by itself entirely explain the NUV properties observed. As suggested for example by Donas et al. (2007; but see also Dorman et al. 1995), who explored slightly different NUV−V correlations, we believe that the above trends result from two main competing effects. On the one hand, young stars have a greater effect in the NUV than the FUV, as only very young stars ($t \lesssim 0.1$ Gyr) can make contributions to the FUV light, while young stars in a much large age range ($t \lesssim 1$ Gyr) contribute to the NUV. Young stars can also influence Hβ for even longer periods ($t \gtrsim 1$ Gyr). As testified by the (NUV−V)–Hβ plot, this is without doubt the reason why the galaxies with a young stellar population are so discrepant. On the other hand, line blanketing (the suppression of the continuum due to a large number of partially overlapping absorption lines) is substantial in the NUV and increases with metallicity. This is probably why the FUV correlations largely disappear in the NUV even for galaxies with no sign of significant recent star formation, as early-type galaxies generally have a high metallicity. Those combined effects probably also explain the lack of correlations in studies which lack a true FUV filter (e.g. Deharveng et al. 2002).
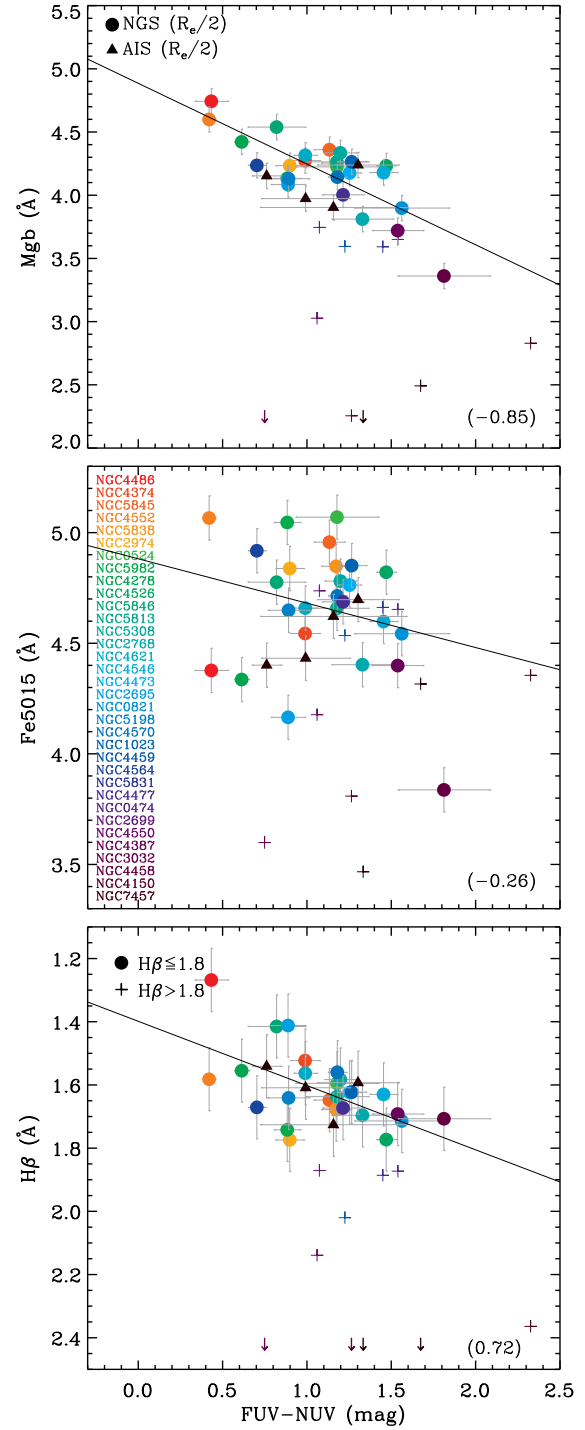
3.5 FUV−NUV

Analogous to Figures 1 and 3, Figure 4 shows the correlations between the FUV−NUV colour and the Mg b, Fe5015 and Hβ linestrength indices. Interestingly, as pointed out especially by Donas et al. (2007), the UV–linestrength correlations are actually much more pronouced and show less scatter when the UV−optical colour FUV−V is replaced by the pure UV colour FUV−NUV. As the metallicity increases, this is most likely due to an increase in the FUV upturn conspiring with increasing line blanketing in the NUV. However, given that the NUV atmospheric opacity is dominated by iron-peak elements, it is surprising that the correlation with Fe5015 is poorer than that with Mg b. As expected, however, the FUV−NUV colours of galaxies with a significant young stellar population are largely uncorrelated
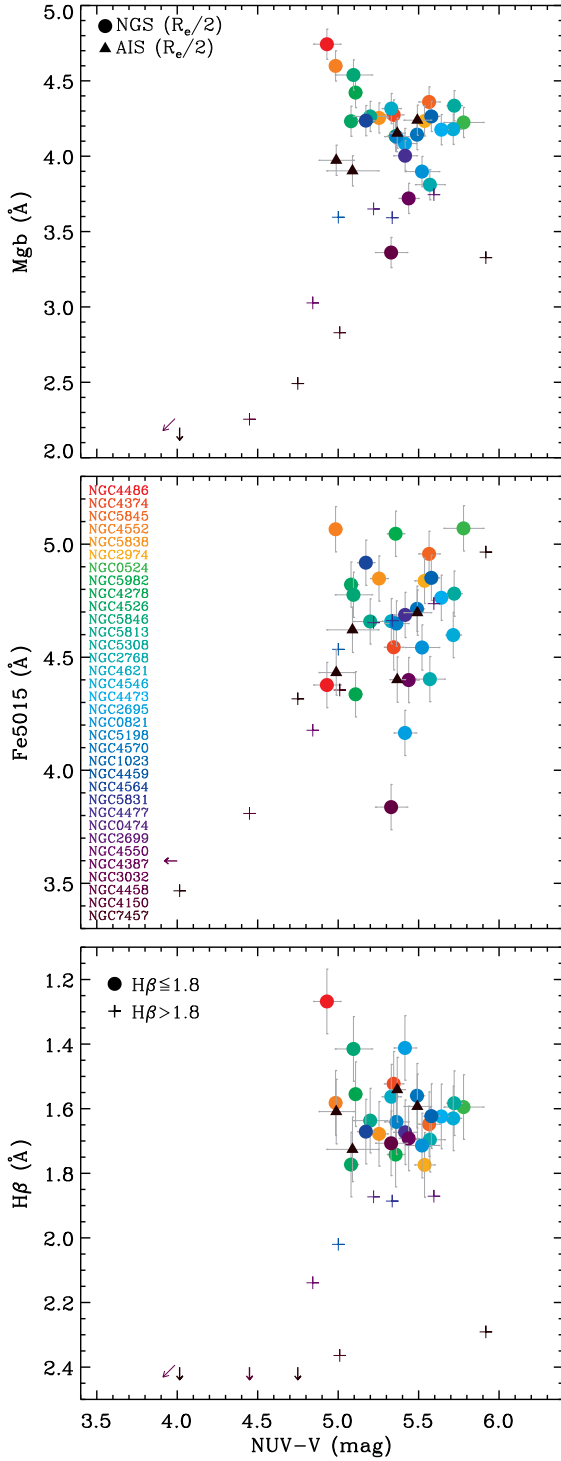
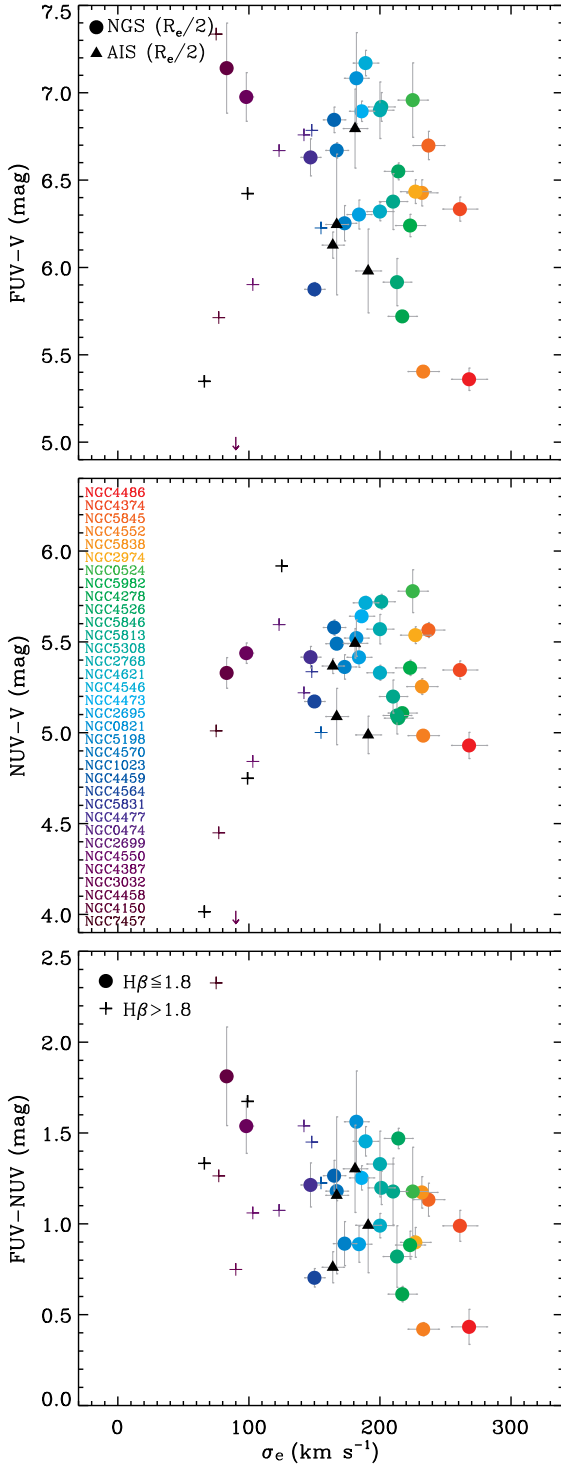**Figure 3.** Same as Figure 1 but for the optical–UV colour (NUV−*V*).

Figure 4. Same as Figure 1 but for the pure UV colour (FUV−NUV).

with the linestrengths. The parameters of the best-fit linear relations are again listed in Table 2.

We stress here that the (FUV−NUV)–Mg*b* correlation is tighter than the Burstein relation, which uses FUV−*V*. Although the Burstein relation has traditionally been used in most work, presumably for historical reasons dating back to BBBFL88, and it remains important, our results suggest that (FUV−NUV)–Mg*b* should instead be the correlation of choice. As FUV and NUV are generally measured with the same instrument, using FUV−NUV rather than FUV−*V* also avoids potential uncertainties in the UV to optical flux calibration.

Figure 5. Same as Figure 1 but for the FUV$-V$, NUV$-V$ and FUV$-$NUV colours as a function of the effective stellar velocity dispersion $\sigma_{\rm e}$.

3.6 Stellar velocity dispersion

The Burstein relation and other correlations highlighted in this paper, combined with the well-known Mg–σ relation (e.g. Terlevich et al. 1981; Bender, Burstein & Faber 1993; Colless et al. 1999; Bernardi et al. 2003), imply a correlation

of the UV-upturn phenomenon with the stellar velocity dispersion, which is a good measure of a galaxy's gravitational potential depth and total mass. The colour scheme in Figures 1, 3 and 4 allows us to gauge this dependence, but only very roughly. It is thus shown explicitly in Figure 5. The corresponding figure showing the dependence of the UV-upturn on the dynamical mass $M_{\rm dyn} \equiv 5.0\,G^{-1}\,R_{\rm e}\,\sigma_{\rm e}^2$ (see Paper IV) is essentially identical. This mass represents $M_{\rm dyn} \approx 2\,M_{1/2}$, where $M_{1/2}$ is the total mass within a sphere containing half of the galaxy light.

Comparing Figures 1 and 5, one can see that the scatter in the Burstein relation is smaller than that in the (FUV$-V$)–$\sigma_{\rm e}$ relation. This effect first pointed out by BBBFL88 lead them to suggest that the UV upturn is primarily driven by stellar population properties rather than structural or dynamical ones. We confirm this trend here. The effect is however much more pronounced when considering the FUV$-$NUV colour, where the correlation with Mg b is very tight but that with $\sigma_{\rm e}$ is much looser. Just as for Mg b, NUV$-V$ does not show any clear dependence on $\sigma_{\rm e}$.

As expected from cosmic downsizing (e.g. Cowie et al. 1996; Treu et al. 2005; Thomas et al. 2005), all galaxies with evidence of recent star formation (high Hβ) are in the low mass half of our sample ($\sigma_{\rm e} \lesssim 180$ km s^{-1}; see also Paper XV).

3.7 Aperture effects

Analogous UV–linestrength correlations to those discussed in this section are also present when using matching elliptical apertures of $R_{\rm e}/8$ and $R_{\rm e}$. The linestrengths and broadband colours are simply slightly offset, as expected from the radial stellar populations gradients present in early-type galaxies. However, some correlations are clearer for smaller apertures. This is most likely because stellar age gradients are generally most pronounced in galaxy centres (e.g. Paper VI; McDermid et al. 2006, hereafter Paper VIII; Paper XVII). The integrated UV$-V$ colours and linestrengths thus have much broader ranges of values for small apertures.

3.8 Multi-dimensional relations

The various correlations shown in Figures 1–5 suggest that Mg b is the dominant parameter affecting the UV flux, but we now consider relations involving three parameters, analogously to the Fundamental Plane for stellar dynamics (relating the stellar luminosity, surface brightness and central velocity dispersion of galaxies; see Djorgovski & Davis 1987; Dressler et al. 1987). Without an a priori physical foundation, such as the virial theorem for the Fundamental Plane, it is however not clear what correlations one should expect. To minimise biases arising from the very different definitions and thus dynamic ranges of the parameters considered (e.g. colours, velocity dispersion and linestrengths), we normalize each parameter to yield an observed range of 1.0. For example, the measured values of FUV$-V$ extend from roughly 5.4 to 7.2 mag (yielding an observed range of 1.8 mag), so in the fits below N(FUV$-V$)= 0.0 mag is actually 1.8 mag bluer (UV stronger) than N(FUV$-V$)= 1.0 mag, where the prefix N denotes a normalised quantity. Likewise for the other quantities (FUV$-$NUV= 0.4–1.8 mag, log($\sigma_{\rm e}$/km s^{-1}) = 1.9–2.4, Mg b = 3.4–4.7 Å, Fe5015 = 3.8–5.1 Å).
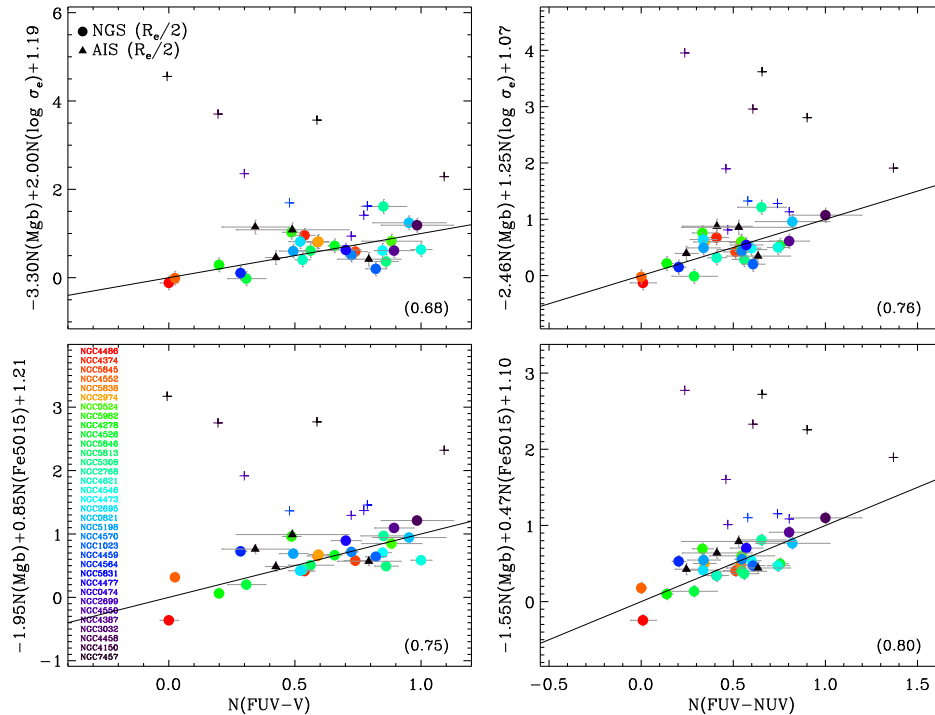
Figure 6. Edge-on views of the best-fit planes for selected three-prameter relations (see text). *Top-left:* Plane relating FUV−V, Mg b and σ_e. *Bottom-left:* Plane relating FUV−V, Mg b and Fe5015. *Top-right:* Plane relating FUV−NUV, Mg b and σ_e. *Bottom-right:* Plane relating FUV−NUV, Mg b and Fe5015. The solid lines are shown to guide the eye and all have slope unity and go through the origin. The correlation coefficient is reported in the bottom-right corner of each panel. The three-parameter correlations shown are not tighter than the two-parameter correlations shown in Figures 1 and 4.

We have explored a number of parameter combinations, but we present only the most promising ones below and in Figure 6, in the sense that the resulting planes (in their respective three-dimensional spaces) are the tightest. The planes were obtained by minimising the square of the residuals in the direction perpendicular the planes, but we warn that the coefficients obtained do depend sensitively on the exact quantity that is minimised. The edge-on projections of the planes are shown in Figure 6. By construction, the solid lines shown (of slope unity and going through the origin) should go through the data points (they do). As before, the fits are performed to the quiescent galaxies only (i.e. $H\beta \leqslant 1.8$ Å), yielding

$$N(FUV - V) = -3.30\,N(Mg\,b) + 2.00\,N(\log \sigma_e) + 1.19\ ,\ (1)$$

$$N(FUV - V) = -1.95\,N(Mg\,b) + 0.85\,N(Fe5015) + 1.21\ ,(2)$$

$$N(FUV - NUV) = -2.46\,N(Mg\,b) + 1.25\,N(\log \sigma_e) + 1.07\ ,(3)$$

$$N(FUV - NUV) = -1.55\,N(Mg\,b) + 0.47\,N(Fe5015) + 1.10\ .(4)$$

The correlation coefficients reported in the bottom right corner of each panel of Figure 6 are no better than those of the good two-parameter fits shown in Figures 1 and 4. None is better than the (FUV−NUV)–Mg b correlation. This implies that the FUV excess is not particularly better described by employing an additional parameter. This is in agreement with our finding of § 3.6, that it is stellar population rather than dynamical properties that govern the UV strength.

4   STAR FORMATION

In the (FUV−V)–linestrength and (FUV−NUV)–linestrength relations discussed in Section 3, the apparent correlations defined by the bulk of the observations are weakened by the presence of a number of outlying data points. However, the outliers systematically have $H\beta > 1.8$ Å, which suggests that the deviations from the bulk are due to the presence of a young stellar component in these galaxies. Indeed, while often negligible in the optical, even a small amount of recent star formation can have a dramatic effect in the UV. We test this hypothesis thoroughly in this section.

Figure 7 shows how the (FUV−NUV)–Mg b correlation measured within $R_e/2$ elliptical apertures depends on a number of star formation tracers, none of which is however perfect. Our best-fit (FUV−NUV)–Mg b relation from Section 3.5 is overplotted as a dashed line for reference. The $H\alpha$ emission line and the mid-infrared (MIR) emission from dust and polycyclic aromatic hydrocarbons (PAHs) are normally considered good tracers of respectively unobscured and obscured ongoing star formation, while the luminosity-weighted mean stellar age traces recent and older star formation events. The molecular gas mass M_{H_2} measures the fuel reserve for current and future star formation. As we must rely on external sources for those quantities, they are not measured within our standard $R_e/2$ aperture, but this is unimportant for the argument. We only use those quantities to gauge the likelyhood of young stars; the data plotted remain measured within identical apertures. The $H\alpha$
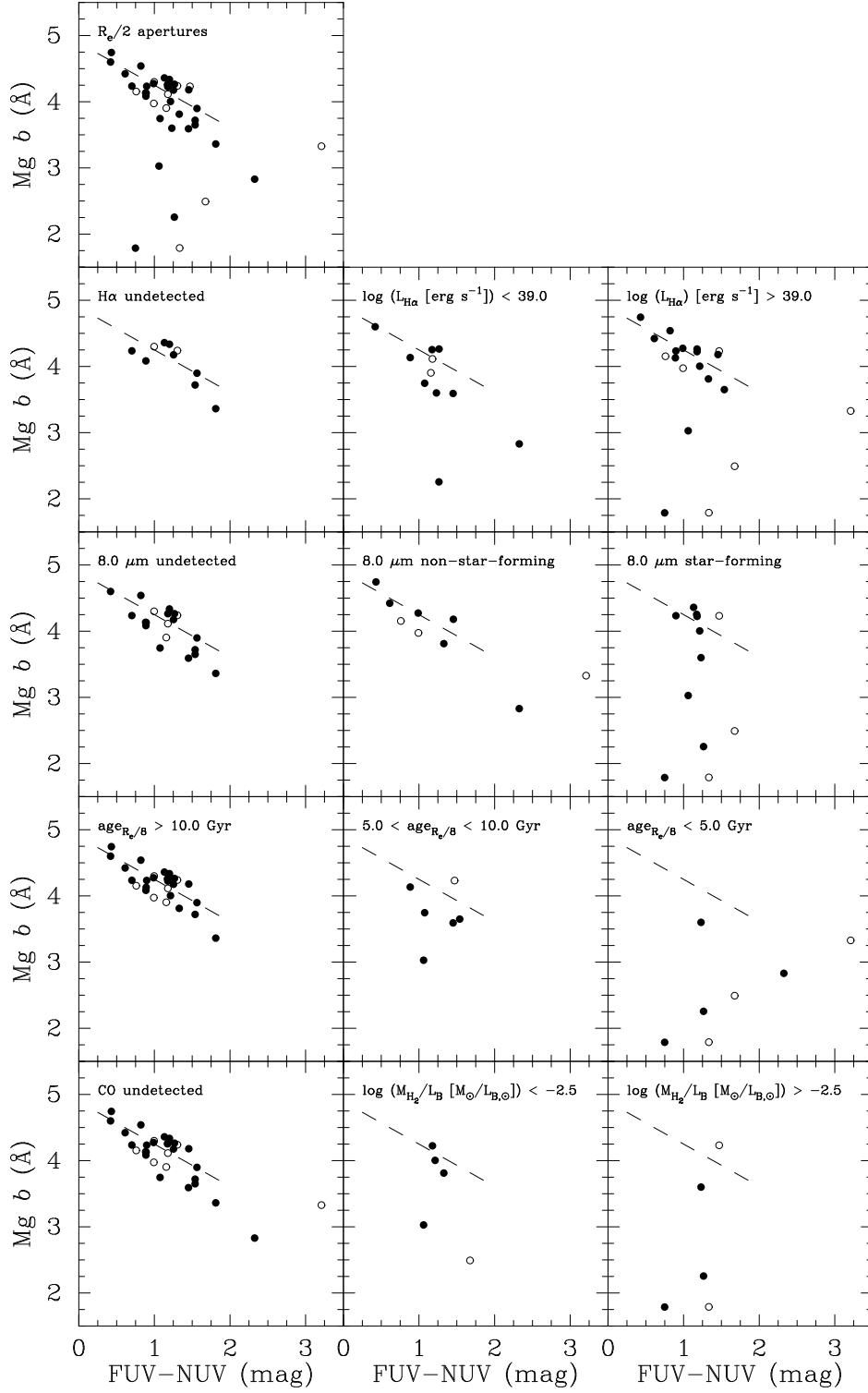
Figure 7. Dependence of the (FUV−NUV)–Mg b correlation on recent and ongoing star formation. The top panel shows the correlation for all galaxies using elliptical apertures of $R_{\rm e}/2$. Lower panels show the correlation as a function of the integrated Hα luminosity, the type of 8.0 μm non-stellar emission if present, the luminosity-weighted mean stellar age and the molecular gas mass normalised by the B-band luminosity. From left-to-right, the columns respectively show galaxies with no, mild or ambiguous, and strong evidence for ongoing or recent star formation. A clear correlation with no outlier is only observed for quiescent galaxies. Filled symbols indicate galaxies with at least one orbit of *GALEX* integration time, while open symbols indicate the shorter exposure AIS data. Error bars have been omitted for clarity and our best-fit (FUV−NUV)–Mg b relation is overplotted as a dashed line for reference.

luminosity is integrated within the SAURON FOV and comes from Paper V. In the MIR, we use the *Spitzer*/Infrared Array Camera (IRAC) 8.0 μm non-stellar emission calculated and discussed in Paper XV. Considering the emission morphology, the radial gradient of the 8.0-to-3.6 μm flux ratio, and the *Spitzer*/Infrared Spectrograph (IRS) spectrum when available, Paper XV very carefully separated the 8.0 μm non-stellar emission originating from star formation and other processes. The mean stellar age is derived through single stellar population synthesis models from linestrengths integrated within a circular aperture of $R_{\rm e}/8$ (Paper XVII). The distance-independent $M_{\rm H_2}/L_B$ ratios are global values and come from the CO measurements of Combes et al. (2007) and Young et al. (2010) combined with the RC3 optical catalogue (de Vaucouleurs et al. 1991).

The main conclusion from Figure 7 is that a clear, tight (FUV$-$NUV)–Mg b correlation without outliers is only present for galaxies which show no sign of current or recent star formation. The scatter is much increased for galaxies with even mild evidence of star formation, and essentially no correlation is present for galaxies with strong evidence. This is particularly nicely illustrated by the mean luminosity-weighted stellar age panels, which show increasing scatter with decreasing mean age.

Other star formation tracers not shown in Figure 7 display analogous behaviours, such as the Hβ absorption linestrength and NUV$-$V colour discussed in this paper, the $B - V$ colour, and the 8.0 μm non-stellar luminosity and associated star formation rate. More importantly, similar results are obtained for other apertures ($R_{\rm e}/8$ and $R_{\rm e}$), FUV$-$V and NUV$-$V colours, and Fe5015 and Hβ linestrengths. In addition, the (FUV$-$V)–(FUV$-$NUV) and (FUV$-$V)–(NUV$-$V) colour-colour relations clearly show that, while the quiescent galaxies (H$\beta \leqslant 1.8$ Å) do define clear correlations (see, e.g., Boselli et al. 2005; Donas et al. 2007), galaxies with evidence of young stars (H$\beta > 1.8$ Å) systematically depart from them. This shows beyond doubt that most deviations from the correlations described in Section 3 are due to galaxies with either current or recent star formation, and that the correlations themselves are essentially due to quiescent galaxies (i.e. purely old stellar populations).

One should not be overly concerned that, occasionally, galaxies with apparent signs of current or recent star formation in Figure 7 do fall within the region expected of our best-fit (FUV$-$NUV)–Mg b relation. As mentioned above, none of the tracers is perfect, especially in early-type galaxies. In particular, as shown in Paper XVI, emission from Balmer lines such as Hα in early-type galaxies is normallly dominated by non-star-formation processes, specifically hot evolved stellar populations (PAGB stars). Absence of Hα emission thus guarantees absence of star formation, but the presence of Hα emission does not imply the presence of star formation. Dust and PAHs can also be heated/ionised by a variety of processes, including these same evolved stellar populations (see Paper XV). A (FUV$-$NUV)–Mg b correlation is only present for galaxies with 8.0 μm non-stellar emission if that emission has a non-star formation origin.

We also note that the scatter in our correlations is not caused by the presence of active galactic nuclei (AGN). First, our measurements are global rather than nuclear. Second, there are only four strong radio continuum sources

in the SAURON sample: two FR I sources (NGC 4374 and NGC 4486), NGC 4278 and NGC 4552. None is particularly discrepant in our correlations. It is clear however that AGN could contribute to the scatter in samples of galaxies constructed differently.

5   SDSS SAMPLE

5.1   Sample selection and data

We now place our findings based on observations of SAURON early-type galaxies in the context of previous work on SDSS galaxies, such as that of Rich et al. (2005). UV and linestrength measurements of SDSS early-type galaxies present a number of challenges. First, most galaxies are invariably unresolved by *GALEX* but the spectral information is derived from SDSS fibre spectra with a 3$''$ diameter, leading to aperture mismatch. Second, except at the highest luminosities, many early-type galaxies in the low-redshift regime ($z \approx 0.05$–0.1) are either undetected or barely detected at the depth of the *GALEX* Medium Imaging Survey (MIS; Martin et al. 2005; Morrissey et al. 2005). Third, a reliable morphological classification is far more challenging. Fourth, disentangling the UV upturn from residual star formation is very difficult.

Given that we do find a correlation between UV$-$optical colours and Mg b in SAURON galaxies, we nevertheless attempt here to overcome these hurdles and show that the Burstein relation pioneered by BBBFL88 can also be found in more distant early-type galaxies, as can other UV–linestrength relations. We use for this purpose the Morphologically Selected Ellipticals in SDSS sample (MOSES; Schawinski et al. 2007), which includes all spectroscopic SDSS galaxies with $r < 16.8$ in the redshift range $0.05 < z < 0.1$ and provides reliable visual morphologies.

The SDSS spectra were first processed with the software GANDALF to remove nebular emission lines (see Paper V), while using pPXF to fit the stellar kinematics (Cappellari & Emsellem 2004). The cleaned spectra were then degraded to the spectral resolution of the Lick indices and stellar absorption linestrengths were measured, including Mg b and Hβ. For details, see Schawinski et al. (2007) and Thomas et al. (2008). With those data in hand, we now address the four challenges listed above.

First, there is no reasonable correction we can apply to the issue of aperture mismatch, so this necessarily remains a source of systematic error for *GALEX*-SDSS galaxies.

Second, since the slope of the Burstein relation is not particularly steep, there is a danger that it could be washed out by large errors in the UV photometry. Even though these requirements substantially reduce the sample size, we thus only consider here those MOSES early-type galaxies that are detected by *GALEX* in *both* NUV and FUV filters, and we further require that the photometric error in each be less than 0.3 mag. These two requirements reduce the sample from 12 828 galaxies for MOSES to 535. Perhaps more importantly, these requirements strongly bias our sample in favour of UV-blue galaxies, particularly compared to the SAURON galaxies discussed in this paper. UV-red galaxies are largely excluded.

Third, it is clear that any automated early-type galaxy

selection criteria based on structural parameters leads to the inclusion of many disc-dominated galaxies, Sa galaxies being a particularly prevalent source of contamination (see, e.g., Schawinski et al. 2007). As galaxies with discs are likely forming stars, they will contaminate the Burstein and other similar relations with UV flux from young stars. The most reliable method for excluding such non-early-type interlopers is visual inspection, which has been carefully performed for the MOSES sample using SDSS images. Short of obtaining space-based data for a substantial number of these galaxies, this is thus the best morphological classification possible.

Fourth, even after removing intermediate and late-type interlopers, residual star formation is still common in low-redshift early-type galaxies (e.g. Yi et al. 2005; Schawinski et al. 2007; Kaviraj et al. 2007), and this residual star formation will dilute the Burstein and other relations. To remove these objects from the sample, it is possible to reject all galaxies with high Hβ linestrengths. Specifically, we investigate here rejecting objects with Hβ + H$\beta_{\rm err}$ > 1.8 Å (see below).

5.2 Burstein relation: FUV−V vs. Mgb

We plot in the top panel of Figure 8 the Mgb linestrength against FUV−g colour for the SDSS early-type galaxies selected. Overplotted is the best-fit Burstein relation derived in Section 3.1, transformed from V to g. The latter correction was obtained using a large sample of early-type galaxies with *GALEX* data selected visually from SDSS. As the $g - V$ colour effectively does not vary with FUV−NUV, we adopted a fixed correction $g - V = 0.53$ mag.

Ignoring the cut on Hβ linestrength, the data in the top panel of Figure 8 only show a loose correlation in a sense opposite to the Burstein relation discussed in Section 3.1. The immense scatter introduced by residual star formation largely washes out the signal in the UV−optical colour. If we however separate the sample according to Hβ linestrength, the picture changes dramatically. Quiescent early-type galaxies with low Hβ values (161 objects with Hβ+H$\beta_{\rm err}$ $\leqslant$ 1.8 Å; black circles) cluster at redder colours and are located roughly within the region expected from the original Burstein relation, with few outliers. Galaxies with a young population with high Hβ values (144 objects with Hβ-H$\beta_{\rm err}$ > 1.8 Å; grey circles) do not and have an entirely different distribution. This selection on Hβ does exclude galaxies whose error bars bestride the Hβ = 1.8 Å threshold between recently star-forming and non-recently star-forming galaxies (i.e. galaxies for which Hβ-H$\beta_{\rm err}$ $\leqslant$ 1.8 Å < Hβ+H$\beta_{\rm err}$), but we believe this is best suited to test our hypothesis that star formation (i.e. the presence of young stars) is mainly responsible for the outliers in the Burstein relation. Galaxies that bridge the threshold may or may not contain young stars and will blur any dichotomy.

Our Hβ criteria are however not perfect discriminants between entirely passive early-type galaxies and those with a low level of residual star formation in the last gigayear. In any case, residual star formation can occur at large radii (see Paper XIII), and this will not be picked up by the SDSS fibres. If we use a blunter selection criterion and restrict ourselves further to early-type galaxies with a high velocity dispersion ($\sigma > 200$ kms^{-1}; 169 of 535 galaxies), where residual
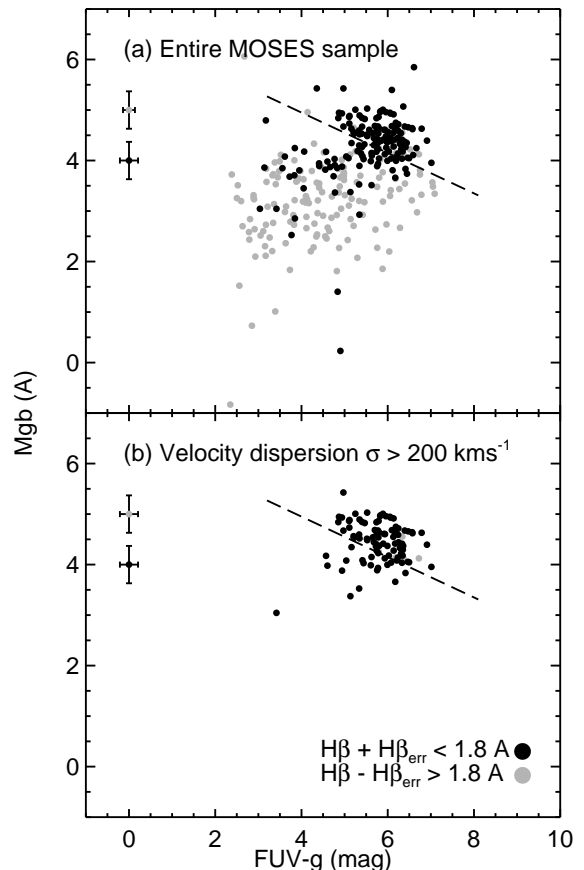
Figure 8. Mg–(FUV−g) relation for the MOSES sample early-type galaxies with good UV photometry. *Top:* Entire sample meeting the Hβ selection criteria. *Bottom:* Only galaxies with a velocity dispersion σ larger than 200 km s^{-1}. Quiescent galaxies with Hβ+H$\beta_{\rm err}$ $\leqslant$ 1.8 Å are shown as black circles, while galaxies consistent with harbouring a young stellar population (Hβ-H$\beta_{\rm err}$ > 1.8 Å) are shown in grey. Characteristic error bars are shown in the top-left of each plot. Our best-fit Burstein relation is overplotted as a dashed line for reference, taking into acount the small $g - V$ colour transformation described in the text.

star formation is virtually completely suppressed (Schawinski et al. 2006, see, e.g.,), then we can see that *all* early-type galaxies cluster within the same locus regardless of the Hβ criteria (see Fig. 8, bottom panel). And indeed, there are very few galaxies with Hβ-H$\beta_{\rm err}$ > 1.8 Å left (5 objects compared to 97 for Hβ+H$\beta_{\rm err}$ $\leqslant$ 1.8 Å). The large errors in both Mgb and FUV−g, in addition to aperture mismatch, result in sufficient scatter to largely hide the (FUV−g)–Mgb relation, but the locus is consistent with the slope and zero-point found for the SAURON galaxies.

Our treatment of the SDSS sample thus supports the presence of (UV−optical)–linestrength relations as described in Section 3.1, but again only for quiescent galaxies. This is true using both an Hβ linestrength (i.e. age) cut and a stellar velocity dispersion (i.e. total mass) cut. Our treatment also illustrates how challenging weeding out galaxies with low levels of residual star formation can be with the data quality typical of large surveys. Here, the sheer num-

ber of galaxies does not trump the need for high quality
data.

6   DISCUSSION

6.1   Origin of the UV upturn

A main result of our work illustrated in Figures 1–4 is that
we recover the Burstein relation for early-type galaxies origi-
nally discussed in BBBFL88, as well as the (NUV−V)–Mg b
and (FUV−NUV)–Mg b correlations discussed in later pa-
pers (e.g. Dorman et al. 1995; Rich et al. 2005; Boselli et al.
2005; Donas et al. 2007). However, contrary to these authors,
we use identical apertures for all quantities. We have also
clearly showed that correlations with the Hβ linestrength
index also exist, albeit usually with larger scatter. Correla-
tions with Fe5015 are at best very weak. These additional
correlations are crucial, as once compared to stellar popula-
tion synthesis models they will allow us to roughly separate
the effects of α-element enhancement, metallicity and age
on the UV-upturn phenomenon (see, e.g., Paper XVII).

Lacking other elements, previous works considered Mg
as a metallicity tracer (e.g. BBBFL88; Rich et al. 2005;
Donas et al. 2007). But given that early-type galaxies and
bulges are known to be over-abundant in α elements (e.g.
Rich 1988; Gorgas, Efstathiou & Aragon Salamanca 1990;
Worthey, Faber & Gonzalez 1992), one might now naively
be tempted to treat Mg primarily as a tracer of α-elements,
and take Fe5015 as the prime metallicity tracer. A high
[α/Fe] ratio is usually interpreted as implying a short star
formation timescale (i.e. a burst), as stars are enriched in
α elements produced by early Type II supernovae but are
not enriched in Fe produced by longer timescale Type Ia
supernovae (e.g. Edvardsson et al. 1993; Fuhrmann 1998;
Thomas, Greggio & Bender 1998). Taken at face-value, the
tight (FUV−V)–Mg b correlation (i.e. the Burstein relation)
would thus suggest that the UV upturn in early-types is pri-
marily due to stars formed in a rapid burst and enriched in
α elements. The extremely loose (FUV−V)–Fe5015 correla-
tion would further suggest that enrichment in Fe produced
over longer timescales is not the primary driver of the cor-
relations. This would then presumably pose challenges to
UV upturn theoretical models with strong metallicity de-
pendences (e.g. EHB models), and equally spell bad news
for scenarios relying on binary star evolution more generally
(e.g. Maxted et al. 2001; Han et al. 2003, 2007).

However, are we really justified to make this simplistic
association of Mg b with α elements and Fe5015 with metal-
licity? The short answer is (un)fortunately no. Although Mg
is an α element, the Mg b index is still primarily driven
by metallicity, while the Fe5015 index includes a number
of poorly understood absorption lines. Furthermore, while
they slightly affect both, α elements dominate neither the
energy generation (He, CNO) nor the atmospheric opacity
(iron-peak elements) in metal-rich galaxies (e.g. Guo et al.
2010). Beside specific spectral features, their effect on UV
light should thus be limited (see also Yi 2008). A proper un-
raveling of the individual effects of α-element enhancement
and metallicity on the UV upturn is thus carried out in the
companion paper by Jeong et al. (in preparation), with the
help of the stellar population synthesis models presented in
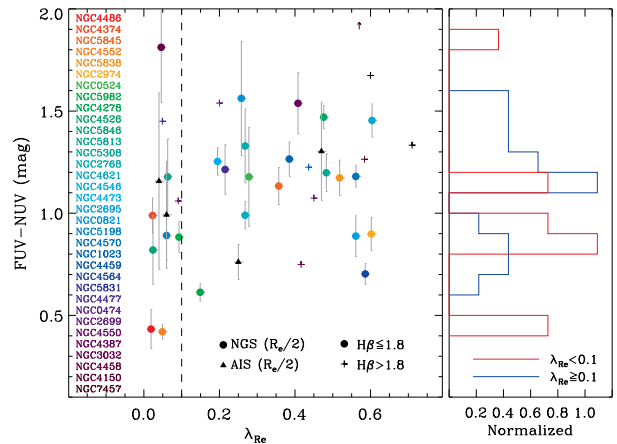
Figure 9. Same as Figure 1 but for the FUV−NUV colour as a
function of the specific angular momentum of the galaxies $\lambda_{\rm R}$. The
normalised number distribution of slow-rotator (red) and fast-
rotator (blue) galaxies as a function of the FUV−NUV colour
is shown on the right for quiescent galaxies only (i.e. cirles and
triangles).

Paper XVII. This is not only the case for the primary de-
pendence of the UV upturn on metallicity, but also for its
dependence on Hβ for old galaxies (H$\beta \leqslant 1.8$ Å). A priori,
this may well be explained entirely by metallicity effects,
but it could also hide a residual age dependence.

Despite having failed to find a dominant dependence
of the UV upturn on $\sigma_{\rm e}$, we can test if other parameters
might better reveal a structural or dynamical influence on
the UV upturn. We find no or weak dependences of the
FUV−V, NUV−V and FUV−NUV colours on the elliptic-
ity ϵ, boxiness of the isophotes a_4 and the ratio of rotational
to pressure support V/σ. In the spirit of recent results of
the SAURON survey, we plot in Figure 9 the dependence of
the UV upturn on $\lambda_{R_{\rm e}}$, the specific angular momentum of
a galaxy measured within $R_{\rm e}$ (see Paper IX for details).
Figure 9 also shows the normalised number distribution of
slow-rotator ($\lambda_{R_{\rm e}} < 0.1$) and fast-rotator ($\lambda_{R_{\rm e}} \geqslant 0.1$) galax-
ies as a function of the FUV−NUV colour, for quiescent
galaxies only. Although there is much scatter, we see that
among quiescent galaxies very blue FUV−NUV colours are
more commonly observed among slow rotators than fast ro-
tators. Clearly, however, more extensive investigations are
necessary to substantiate any dynamical dependence of the
UV upturn.

Lastly, we point out that the scatter in the UV–
linestrength relations presented here (e.g. the Burstein rela-
tion) is larger than our measurement errors. It is thus real,
implying that there is not a one-to-one correlation between
the UV excess and absorption linestrengths. This is an im-
portant result, but stellar evolution models of course do not
depend on linestrengths but rather on age, metallicity and
α-element abundance.

6.2   Star formation

Our work shows that star formation is responsible for most
outliers in the UV–linestrength correlations. Indeed, with
the extensive ancillary data available for the SAURON sample,

and the exquisite sensitivity reached for nearby objects, we were able to systematically identify all outliers with galaxies showing signs of recent or current star formation. This could also be done in an analogous manner for a much larger (and more distant) sample of galaxies from SDSS. The fact that clear correlations are then only recovered for massive galaxies with high quality data can probably be explained by the relative poor sensitivity of SDSS to the presence of recent and/or current star formation (more likely present in low-mass systems).

The same reason probably explains the results of Rich et al. (2005), which are most at odds with those of BBBFL88. We support here the results of Donas et al. (2007), who argued in favour of contamination from low-level star formation in their own sample, especially for the lenticulars. Requiring $S/N \geqslant 10$ for the SDSS spectra (although they quote a final $S/N = 23 \pm 7$ for their quiescent sample), Rich et al. (2005) were probably not as sensitive to weak emission lines and thus star formation as we are here. It would be interesting to see the UV−optical colour corresponding to their Hα emission (and thus star formation) upper limits. We require here $S/N \geqslant 60$ per spatial bin (and spectral element) for SAURON and simultaneously fit both absorption and emission lines, yielding an equivalent width sensitivity of 0.1 Å (see Paper V). We also have much ancillary data, including the age-sensitive Hβ absorption line index.

We also stress here a fact that has generally been overlooked in previous UV-upturn observational studies. All galaxies which are off the relations, and which we identify as having current or recent star formation in Sections 4 and 5, are systematically below the correlations. That is, they systematically have Mg b and Fe5015 linestrengths which are lower than those predicted by the correlations for purely old galaxies. None has significantly higher Mg b or Fe5015, and the effect is particularly pronounced for Mg b. Considering the predictions of stellar population synthesis models (e.g. Thomas et al. 2003), this is entirely consistent with the outliers being of systematically lower mean ages.

7 CONCLUSIONS

We have used space-based UV ultraviolet photometry from *GALEX*, ground-based optical photometry from MDM and ground-based optical integral-field spectroscopy from SAURON to study the UV–linestrength relations of early-type galaxies. Focusing on the SAURON sample, those data represent significant improvements over previous work. In particular, identical apertures could be used for all datasets, eliminating the aperture mismatch issues that have affected previous studies.

We have shown that early-type galaxies follow fairly tight correlations between the integrated FUV−V and FUV−NUV colours and the integrated Mg b and Hβ linestrength indices, less so for the NUV−V colour, Fe5015 index and stellar velocity dispersion σ. Through stellar population synthesis models, these correlations constrain the dependence of the UV-upturn phenomenon in early-type galaxies on age, metallicity and α-element abundance. In particular, despite some recent controversy stemming from the analysis of large survey datasets, we have recovered a (FUV−V)–Mg b correlation that is analogous and entirely

consistent with that first proposed by BBBFL88. We refer to this and the original relation as the Burstein relation. This relation clearly suggests a positive dependence of the UV-upturn on metallicity and is stronger when the pure UV colour (FUV−NUV) is used, although any possible dependence on age must await a better comparison with models. The scatter in the correlations appears to be real and there is mild evidence that a strong UV excess is preferentially present in slow-rotating galaxies, although this last point deserves further study.

Using ancillary data constraining past and current star formation in our sample galaxies, we have shown that most data that do not follow the main correlations can be attributed to galaxies with evidence for recent star formation, even if weak. The UV–linestrength correlations discussed thus appear to hold exclusively for old stellar populations. A large sample of more distant early-type galaxies selected from SDSS, and thus easier to relate to current large surveys, supports this view. The same can be said of the correlations outliers themselves, which have systematically lower Mg b, Fe5015 and higher Hβ linestrength indices.

Given that galaxies show internal colour and linestrength gradients, it is natural to ask whether the global correlations observed here also apply locally within galaxies. Using the full capabilities accorded to us by integral-field data, this issue is the focus of a companion paper (Jeong et al., in preparation).

REFERENCES

Bender R., Burstein D., Faber S. M., 1993, ApJ, 411, 153

Bernardi M., et al., 2003, AJ, 125, 1882

Bertola F., Capaccioli M., Holm A. V., Oke J. B., 1980, ApJL, 237, L65

Boselli A., et al., 2005, ApJ, 629, L29

Bressan A., Chiosi C., Fagotto F., 1994, ApJS, 94, 63

Brown T. M., 2004, Ap&SS, 291, 215

Brown T. M., Ferguson H. C., Davidsen A. F., Doorman B., 1997, ApJ, 482, 685

Burstein D., Bertola F., Buson L. M., Faber S. M., Lauer T. R., 1988, ApJ, 328, 440 [BBBFL88]

Burstein D., Davies R. L., Dressler A., Faber S. M., Lynden-Bell D., 1988, in Towards understanding galaxies at large redshift (Dordrecht: Kluwer Academic Publishers), p. 17

Buzzoni A., González-Lópezlira R. A., 2008, ApJ, 686, 1007

Cappellari M., Emsellem E., 2004, PASP, 116, 138

Cappellari M., et al., 2006, MNRAS, 366, 1126 [Paper IV]

Cappellari M., et al., 2007, MNRAS, 379, 418 [Paper X]

Cardelli J. A., Clayton G. C., Mathis J. S., 1989, ApJ, 345, 245

Code A. D., Welch G. A., Page T., 1972, in Code A. D., ed., Scientific Results from the Orbiting Astronomical Observatory (OAO-2). NASA SP-310, p. 559

Code A. D., Welch G. A., 1979, ApJ, 228, 95

Colless M., Burstein D., Davies R. L., McMahan R. K., Saglia R. P., Wegner G., 1999, MNRAS, 303, 813

Combes F., Young L. M., Bureau M., 2007, MNRAS, 377, 1795

Cowie L. L., Songaila A., Hu E. M., Cohen J. G., 1996, AJ, 112, 839

Crocker A. F., Bureau M., Young L. M., Combes F., 2010, MNRAS, in press

Djorgovski S., Davis M., 1987, ApJ, 313, 59

Deharveng J.-M., Boselli A., Donas J., 2002, A&A, 393, 843

de Vaucouleurs G., de Vaucouleurs A., Corwin H. G., Buta R. J., Paturel G., Fouque P., 1991, *Third Reference Catalogue of Bright Galaxies* (Springer-Verlag: New York)

de Zeeuw P. T., et al., 2002, MNRAS, 329, 513 [Paper II]

Donas J., et al., 2007, ApJS, 173, 597

Dorman B., O'Connell R. W., Rood R. T.,1995, ApJ, 442, 105

Dressler A., Lynden-Bell D., Burstein D., Davies R. L., Faber S. M., Terlevich R., Wegner G., 1987, ApJ, 313, 42

Edvardsson B., Andersen J., Gustafsson B., Lambert D. L., Nissen P. E., Tomkin J., 1993, A&A, 275, 101

Emsellem E., et al., 2004, MNRAS, 352, 721 [Paper III]

Emsellem E., et al., 2007, MNRAS, 379, 401 [Paper IX]

Faber S. M., 1983, Highlights of Astronomy, 6, 165

Faber S. M., Friel E. D., Burstein D., Gaskell C. M., 1985, ApJS, 57, 711

Ferreras I., Silk J., 2000, ApJ, 541, L37

Fuhrmann K., 1998, A&A, 338, 161

Gil de Paz A., et al., 2007, ApJS, 173, 185

Gorgas J., Efstathiou G., Aragon Salamanca A., 1990, MNRAS, 245, 217

Greggio L., Renzini A., 1990, ApJ, 364, 35

Guo J., Zhang F., Zhang X., Han Z., 2010, Ap&SS, 51, in press

Han Z., Podsiadlowski Ph., Lynas-Gray A. E., 2007, MNRAS, 380, 1098

Heber U., 2009, ARA&A, 47, 211

Han Z., Podsiadlowski Ph., Maxted P. F. L., Marsh T. R., 2003, MNRAS, 341, 669

Horch E., Demarque P., Pinsonneault M., 1992, ApJ, 388, L53

Jeong H., et al., 2009, MNRAS, 398, 2028 [Paper XIII]

Kaviraj S., Sohn S. T., O'Connell R. W., Yoon S.-J., Lee Y.-W., Yi S. K., 2007, MNRAS, 377, 987

Kaviraj S., et al., 2007, ApJS, 173, 619

Kuntschner H., et al., 2006, MNRAS, 369, 497 [Paper VI]

Kuntschner H., et al., 2010, MNRAS, 408, 97 [Paper XVII]

Landolt A. U., 1992, AJ, 104, 340

Lee Y.-W., Demarque P., Zinn R., 1994, ApJ, 423, 248

Lee Y.-W., Gim H. B., Casetti-Dinescu D. I., 2007, ApJ, 661, L49

Lee Y.-W., et al., 2005a, ApJ, 619, L103

Lee Y.-W., et al., 2005b, ApJ, 621, L57

Martin D. C., et al., 2005, ApJ, 619, L1

Maxted P. F. L., Heber U., Marsh T. R., North R. C., 2001, MNRAS, 326, 1391

McDermid R. M., et al., 2006, MNRAS, 373, 906 [Paper VIII]

Morrissey P., et al., 2005, ApJ, 619, L7

O'Connell R. W., 1999, ARA&A, 37, 603

Park J.-H., Lee Y.-W., 1997, ApJ, 476, 28

Ree C. H., et al., 2007, ApJS, 173, 607

Rich R. M., 1988, AJ, 95, 828

Rich R. M., et al., 2005, ApJL, 619, L107
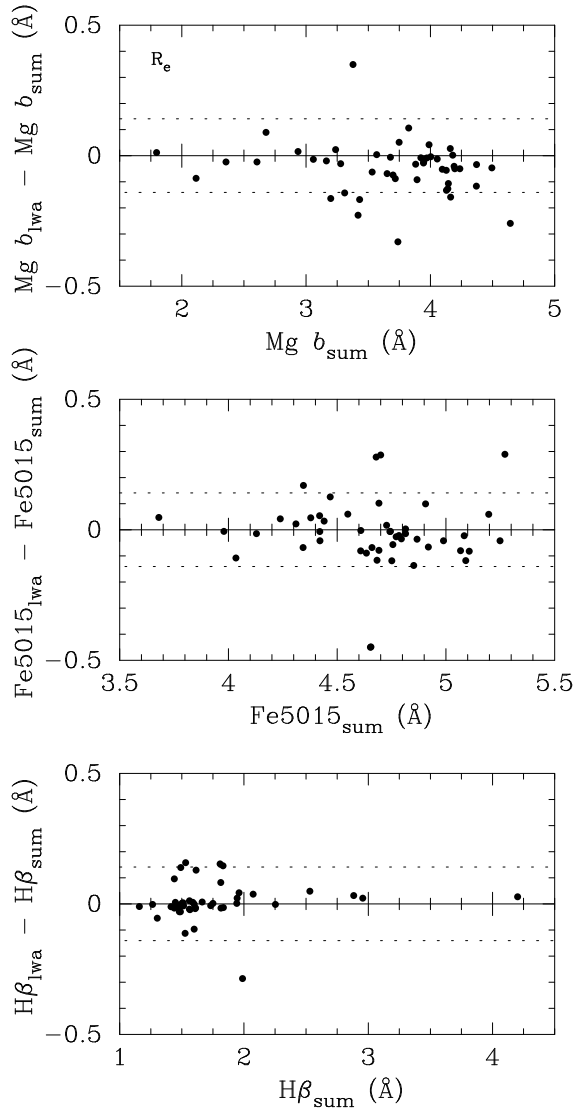
Sarzi M., et al., 2006, MNRAS, 366, 1151 [Paper V]

Sarzi M., et al., 2010, MNRAS, 402, 2187 [Paper XVI]

Schawinski K., Thomas D., Sarzi M., Maraston C., Kaviraj S., Joo S.-J., Yi S. K., Silk J., 2007, MNRAS, 382, 1415

Schawinski K., et al., 2006, Nature, 442, 888

Schawinski K., et al., 2007, ApJS, 173, 512

Schiavon R. P., 2007, ApJS, 171, 146

Schlegel D. J., Finkbeiner D. P., Davis M., 1998, ApJ, 500, 525

Scott N., et al., MNRAS, 2009, 398, 1835 [Paper XIV]

Shapiro K. L., et al., 2010, MNRAS, 402, 2140 [Paper XV]

Sohn S. T., O'Connell R. W., Kundu A., Landsman W. B., Burstein D., Bohlin R. C., Frogel J. A., Rose J. A., 2006, AJ, 131, 866

Temi P., Brighenti F., Mathews W. G., 2009, ApJ, 695, 1

Terlevich R., Davies R. L., Faber S. M., Burstein D., 1981, MNRAS, 196, 381

Thomas D., Greggio L., Bender R., 1998, MNRAS, 296, 119

Thomas D., Maraston C., Bender R., 2003, MNRAS, 339, 897

Thomas D., Maraston C., Bender R., Mendes de Oliveira C., ApJ, 621, 673

Thomas D., Maraston C., Schawinski K., Sarzi M., Joo S.-J., Kaviraj S., Yi S. K., Silk J., 2009, MNRAS, submitted

Treu T., Ellis R. S., Liao T. X., van Dokkum P. G., 2005, ApJL, 622, L5

Worthey G., Faber S. M., Gonzalez J. J., 1992, ApJ, 398, 69

Yi S. K., 2003, ApJ, 582, 202

Yi S. K., 2008, in Heber U., Jeffery C. S., Napiwotzki R., eds., Hot Subdwarf Stars and Related Objects, ASP: San Francisco, 3

Yi S., Demarque P., Kim Y.-C., 1997, ApJ, 482, 677

Yi S., Lee Y.-W., Woo J.-H., Park J.-H., Demarque P., Oemler A. Jr., 1999, ApJ, 513, 128

Yi S. K., Yoon S.-J., 2004, Ap&SS, 291, 205

Yi S. K., et al., 2005, ApJL, 619, 111

Young L. M., et al., 2010, MNRAS, submitted

APPENDIX A: AVERAGE LINESTRENGTH MEASUREMENTS

Formally, to measure the average linestrength within a `SAURON` aperture containing multiple bins, we should sum the (fully calibrated) spectra of all the bins within that aperture and re-measure the linestrength. However, recalculating the linestrength implies re-deriving the stellar kinematics, re-subtracting the ionised gas emission, re-correcting the linestrength for velocity broadening, etc, as done in Paper VI. It is thus a time-consuming task. Furthermore, in a companion paper exploring the UV–linestrength relations as a function of radius within individual galaxies (Jeong et al., in preparation), we integrate the linestrengths over elliptical annuli (rather than elliptical apertures). The resulting LOSVDs can then be significantly non-Gaussian, which makes the stellar kinematic and velocity dispersion correction calculations problematic. It is thus preferable to find a method to integrate (i.e. average) the linestrengths in an aperture using the linestrength measurements in individual bins themselves.

In Figure A1, we show the properly averaged

linestrength measurements of Paper XVII within a circular aperture of radius R_e, compared to measurements obtained by simply averaging the linestrength values of the individual bins within that same aperture, weighted by the luminosity of each bin. While there is some scatter, it is much smaller than the range of values covered, the difference between the two measurements is always small, typically less than the error on each measurement (Paper XVII quotes a formal random uncertainty on integrated linestrengths of at most 0.1 Å, and we have adopted the same uncertainty on our measurements here), and the few outliers systematically have very large effective radii. Most importantly, there is no significant trend with the linestrength values themselves. An aperture of R_e is also the worst case scenario, and even smaller differences are obtained for smaller apertures involving fewer bins. It thus seems that, although not formally equivalent, simple luminosity-weighted linestrength averages do yield accurate estimates. We have thus adopted this averaging method for `SAURON` papers requiring integrated linestrength values (e.g., Scott et al. 2009, hereafter Paper XIV; Jeong et al., in preparation).

Figure A1. Comparison of integrated linestrength values obtained by properly summing the spectra (labeled "sum") and simply luminosity-weighting the linestrength values themselves (labeled "lwa") within circular apertures of radii R_e. Error bars are omitted for clarity, but the adopted formal random error on either quantity is 0.1 Å. *Top:* Mg b. *Middle:* Fe5015. *Bottom:* Hβ. The scatter is always much smaller than the range of values covered and there is no significant systematic trend. The dotted lines show the 0.14 Å formal random error on the difference.